

Evaluation of Viscoelastic Contact Effects on Grasping

Abstract—Viscoelasticity is a common contact characteristic found in humanoid robot skin and soft grippers. Due to its time-dependent nature, viscoelastic properties complicate the response behavior at the contact interface and alter the impedance and stability during grasping. However, studies on the impact of viscoelastic contact on grasp quality remain limited. This article proposes a method for evaluating the effects of viscoelasticity on robotic grasping based on contact modeling. A mathematical model is established to describe the contact stiffness of the viscoelastic interface, and a generalized grasp stiffness matrix is constructed to characterize impedance in different directions. From this, three metrics are derived to evaluate grasp quality, and their physical meanings are discussed. Simulations and robotic experiments are conducted to demonstrate and validate grasp evaluation cases using the proposed method. Finally, three major influences of viscoelasticity on grasping are summarized, providing new perspectives on enhancing grasp performance through viscoelastic characteristics.

I. INTRODUCTION

Grasping plays a vital role across various robotic application domains, including factories and home environments [1]–[4]. In these unstructured settings, object properties and external contact conditions are often unpredictable [5]. To ensure high stability and affordance, robots are expected to autonomously select appropriate grasp configurations, such as grasp postures and forces, through sensing and planning. This requires robots to be capable of evaluating grasp candidates based on effective quantitative metrics, i.e., the quality of grasping [6], [7]. High-quality grasps not only enable the object to resist external disturbances but also help avoid damage and maintain operational flexibility [8]. Therefore, grasping evaluation has long been a critical issue in the robotic community [9].

Traditionally, robotic end-effectors are made of rigid components to ensure precision and load-bearing capacity. As a result, rigid point contact models are typically adopted to simplify analysis. Researchers have proposed a variety of grasp quality metrics, including those based on contact locations, hand configurations, or a combination of both [9], [10]. Some approaches formulate the grasp planning problem as an optimization of a quality function, based on form and force closures [11], [12]. For instance, grasp metrics based on the grasp wrench space (GWS) quantify the quality of force-closure grasps [13], [14]. Besides, generalized grasp matrices based on contact mechanics are widely used to construct features such as potential energy or singular values for grasp evaluation [15], [16]. A common feature of the above methods is their focus on evaluating static force transmission, as rigid contacts assumes point contact and no deformation. Accordingly, these approaches often adopt static metrics and Coulomb friction in constructing the contact mechanics.

Conventional rigid grippers are well-suited for industrial scenarios requiring high load capacity and precision, but lack the adaptability and safety required for applications in daily life [17]. In recent years, soft material-based grippers have increasingly been applied in unstructured tasks, raising new demands for contact modeling [18], [19]. Soft contact components possess compliance similar to human skin, thereby enabling passive adaptation to object shapes and enhancing high stability. With the diversification of fingertip materials, robotic fingertips exhibit viscoelastic behavior under dynamic loads [20], [21], akin to the human behavior. Meanwhile, studies indicate that soft fingertips with viscoelastic properties can improve manipulation and grasping capabilities [22]. As a result, modeling viscoelasticity is essential for advancing quantitative grasping control.

While viscoelasticity enriches the possible contact modes, it also introduces challenges in modeling. Compared to elastic contact, the response of viscoelastic contact depends on multiple factors such as loading rate, direction, and grasp posture. Also, the stress and strain characteristics of viscoelastic materials vary over time and are difficult to solve in closed form, which may affect stiffness and stability during the grasping [23]–[25]. Although some studies have explored mechanical models of viscoelastic contact [20], [26] and conducted experimental investigations [23], [24], there remains a lack of sufficient research quantitatively analyzing the impact of viscoelastic contact on grasping, particularly in establishing a contact stiffness matrix directly related to grasp quality [7], [27], [28]. Given that existing grasp quality evaluation methods typically focus on rigid point or patch contacts, representing and assessing viscoelastic contact behavior remains an open problem.

In this article, we propose a model to evaluate the impact of viscoelastic contact on grasping. The method constructs a generalized stiffness matrix and three evaluation metrics based on a viscoelastic contact model. Using the proposed evaluation approach, case studies analyze the relationship between grasp quality and factors such as contact surface viscosity, load application time, and grasp configurations. Robot experiments validate the effectiveness of the method. Finally, we summarize the main effects of viscoelastic contact to guide grasp control using viscoelastic fingertips.

The remainder of this article is organized as follows: Section II introduces the viscoelastic contact modeling and the construction of the grasp stiffness matrix. Three evaluation metrics along with their physical meanings have been discussed. In Section III, we present three typical case studies analyzing the impact of viscoelastic contact on grasping. Section IV shows experiments on the real robot to further validate the effectiveness of the proposed method. Finally, Sections V and VI provide discussion and conclusions.

II. METHODOLOGY

A. Viscoelastic Contact Model

In typical grasping and manipulation tasks, the directly controlled variable is usually the grasp force (e.g., maintaining a certain grasp force to hold an object or adjusting the force to prevent slippage) rather than contact deformation [20]. Therefore, creep is a primary effect considered in grasping tasks. The viscoelastic properties of a fingertip are examined using the generalized Kelvin model [29], [30]. As shown in Fig. 1(a), the generalized Kelvin model consists of multiple Kelvin elements connected in series, with springs and dashpots representing the elastic and viscous properties of the material, respectively. Let E_i^K and τ_i^K denote the creep modulus and time of the i -th order element (τ_i^K is the ratio of viscosity η_i^K to modulus E_i^K), where m is the total number of orders. Considering a constant stress f , according to [20], [29], the strain in the generalized Kelvin model is given by:

$$u(t) = f \cdot \sum_{i=1}^m \frac{1}{E_i^K} \left(1 - e^{-\frac{t}{\tau_i^K}}\right). \quad (1)$$

Considering the elastic component, let E_0 denote the instantaneous elastic modulus. Then, the fingertip's creep modulus in the time domain is expressed as:

$$E(t) = \left[\frac{1}{E_0} + \sum_{i=1}^m \frac{1}{E_i^K} \left(1 - e^{-\frac{t}{\tau_i^K}}\right) \right]^{-1}. \quad (2)$$

In practice, the viscoelastic properties of materials are typically characterized by relaxation experiments and represented as a Prony series [31]. Therefore, combinations of multiple Maxwell elements are more widely used to describe viscoelastic materials [see Fig. 1(b)]. However, constructing an analytical solution of the creep modulus directly from the generalized Maxwell model is challenging. Considering that related studies have demonstrated the equivalence between the generalized Maxwell and generalized Kelvin models [32], [33], this article attempts to provide the time-domain expression of the elastic modulus based on material parameters from the generalized Maxwell model.

Let E_i^M and η_i^M denote the relaxation modulus and viscosity of the i -th element in an m -order Maxwell model, respectively. Accordingly, each Maxwell branch satisfies the following function:

$$Du = \left(\frac{1}{\eta_i^M} + \frac{D}{E_i^M} \right) f_i, \quad i \in \{1, 2, \dots, m\}, \quad (3)$$

where D is the differential operator. If a Kelvin model (E_0, η_0) is connected in parallel to this model, the overall stress-strain relationship satisfies the constraint:

$$f = \sum_{i=1}^m f_i + (E_0 + \eta_0 D)u. \quad (4)$$

Based on Eqs. (3) and (4), the creep differential equation of the model can be established as follows:

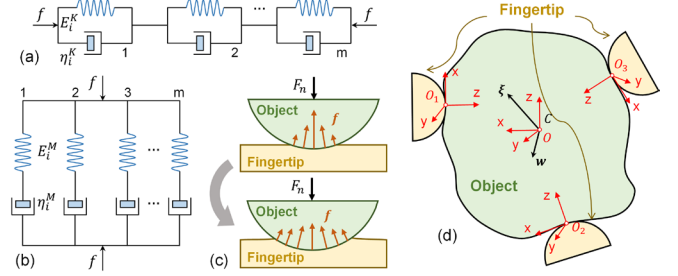


Fig. 1. Viscoelastic contact model. (a) Generalized Kelvin models in series [29]. (b) Generalized Maxwell models in parallel [29]. (c) Evolution of distributed forces and growth of contact area on the viscoelastic contact interface under fixed normal force. (d) 2-D multi-fingertip grasping framework.

$$\prod_{i=1}^m \left(\frac{1}{E_i^M} D + \frac{1}{\eta_i^M} \right) f = D \sum_{i=1}^m \prod_{j=1, j \neq i}^m \left(\frac{1}{E_j^M} D + \frac{1}{\eta_j^M} \right) u + (E_0^M + \eta_0^M D) \prod_{i=1}^m \left(\frac{1}{E_i^M} D + \frac{1}{\eta_i^M} \right) u. \quad (5)$$

According to [32], the resulting generalized Maxwell model can be equivalently represented as a generalized ($m+1$)-order Kelvin model, with the equivalence relation established as:

$$\begin{cases} E_i^K = \eta_0^M \frac{\alpha_i}{\beta_i}, \\ \eta_i^M = \eta_0^M \frac{1}{\beta_i}, \end{cases} \quad i \in \{1, 2, \dots, m+1\}. \quad (6)$$

In Eq. (6), α_i denotes the $m+1$ roots of the polynomial

$$\bar{Q}(s) = \prod_{i=1}^m \eta_i^M \cdot \left[\begin{array}{c} \prod_{i=1}^m \left(\frac{1}{\eta_i^M} - \frac{1}{E_i^M s} \right) (E_0 - \eta_0 s) \\ - \sum_{i=1}^m \prod_{j=1, j \neq i}^m \left(\frac{1}{\eta_j^M} - \frac{1}{E_j^M s} \right) s \end{array} \right], \quad (7)$$

in the complex domain, and

$$\beta_i = \frac{\prod_{j=1}^m (E_j^M / \eta_j^M - \alpha_i)}{\prod_{j=1, j \neq i}^{m+1} (\alpha_j - \alpha_i)}. \quad (8)$$

According to [32], $\alpha_i > 0$ and $\beta_i > 0$ hold true, so the model satisfies a stress-strain relationship similar to the form of Eq. (1). For the case studied in this article, η_0^M should approach zero. Tests show that when η_0^M is chosen sufficiently small, the numerical results of $\{E_i^K\}$ and $\{\eta_i^M\}$ converge, and the contact modulus does not diverge. Therefore, based on Eqs. (1) and (6), the fingertip's creep modulus is expressed as:

$$E(t) = E_0 \cdot g(t), \quad (9)$$

$$g(t) = \lim_{\eta_0 \rightarrow 0} \left[1 + \sum_{i=1}^{m+1} \frac{E_0 \beta_i}{\eta_0 \alpha_i} (1 - e^{-\alpha_i t}) \right]^{-1}. \quad (10)$$

$g(t)$ is defined as the viscoelastic effect function, reflecting the influence of material viscosity on the creep

TABLE I
MATERIAL PARAMETERS OF VHB 4910 [32]

S_0 (kPa)	S_1^M (kPa)	S_2^M (kPa)	S_3^M (kPa)	S_4^M (kPa)
13.65	120.78	37.02	7.061	13.155
	S_1^M (s)	τ_2 (s)	τ_3 (s)	τ_4 (s)
	120.78	37.02	7.061	13.155

modulus. Taking the actual measured parameters of the VHB 4910 viscoelastic material shown in Table I [31] as an example, a 4th-order generalized Maxwell model is established to analyze the characteristics of $g(t)$. Here, S denotes the shear modulus, which can be converted to the elastic modulus by $E = 2(1 + \nu)S$. Based on experience, the Poisson's ratio is assumed to be $\nu = 0.48$, and $\eta_0 = 10^{-8}$ is selected. Meanwhile, a viscosity coefficient γ is introduced to uniformly scale the creep time terms of each order, considering the effect of viscosity variations on $g(t)$:

$$g_\gamma(t) = \lim_{\eta_0 \rightarrow 0} \left[1 + \sum_{i=1}^{m+1} \frac{E_0 \beta_i}{\eta_0 \alpha_i} \left(1 - e^{-\frac{\alpha_i t}{\gamma}} \right) \right]^{-1}. \quad (11)$$

The plot of $g(t)$ is shown in Fig. 2. The results indicate that the creep modulus gradually decreases over time, but the rate of change slows down from large to small. Ultimately, it converges to the equilibrium modulus

$$E_\infty = \lim_{\eta_0 \rightarrow 0} \left[1 + \sum_{i=1}^{m+1} \frac{E_0 \beta_i}{\eta_0 \alpha_i} \right]^{-1}. \quad (12)$$

Here, the greater the viscosity, the faster the creep modulus decreases. Although the same elastic modulus is chosen, when the viscosity differs by a factor of 4, the creep modulus shows up to a 12% deviation after 10 seconds. Additionally, for VHB 4910, the change rate of the creep modulus significantly slows down after about 1 second. Therefore, the viscoelastic effect of this material is mainly reflected in the early stage of the creep process.

B. Contact Stiffness

Consider a semi-elastic space and Hertzian contact, and introduce the Winkler model (a 2-d model) as a substitute for the 3-d continuous medium [34]. Assume that the contact interface always operates within the friction limit to focus on the variation of grasp impedance. For elastic contact under this simplified model, the normal stiffness, tangential stiffness, and torsional stiffness can be expressed as [7], [34]:

$$\begin{cases} K_n = \frac{2aE}{1-\nu^2} \\ K_t = \frac{4aS}{2-\nu} \\ K_m = \frac{16}{3}a^3S \end{cases}, \quad (13)$$

where a represent the contact area.

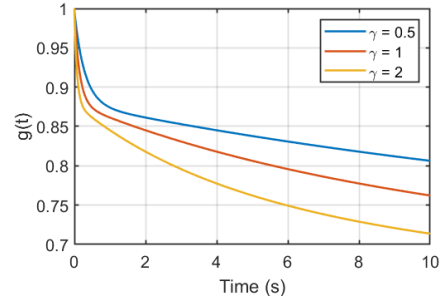


Fig. 2. Variation of the viscoelastic effect function $g(t)$ over time. Material parameters are taken from [31], and viscosity coefficients are artificially set to compare the impact of viscosity on stiffness.

Assuming the material is isotropic, thus $g(t)$ is identical in all directions. Meanwhile, both normal and tangential loading are applied simultaneously. For the case of viscoelastic contact, one factor that must be considered is the variation in contact geometry. As shown in Fig. 1(c), when the normal displacement response increases over time due to the influence of the creep compliance, the contact area also expands. Under the assumption of Hertzian contact, the relationship between the radius of the circular contact area and the displacement is constructed according to [20]:

$$a(t) = a_0 \sqrt{\frac{u_n(t)}{u_n(0)}} = \frac{a_0}{\sqrt{g(t)}}, \quad (14)$$

$$\text{where } a_0 = \left[\frac{3(1-\nu^2)F_n R}{4E_0} \right]^{\frac{1}{3}}, \quad (15)$$

a_0 denotes the instantaneous contact radius (i.e., the contact area in the absence of viscosity), F_n is the normal force, and R is the curvature radius of the contact surface. Building upon Eq. (13), the derivation result from Eq. (9) is incorporated as:

$$K_n(t) = \frac{2a(t)E(t)}{1-\nu^2} = \frac{2a_0 E_0}{1-\nu^2} \cdot \sqrt{g(t)}, \quad (16)$$

$$K_\tau(t) = \frac{4a(t)S(t)}{2-\nu} = \frac{2a_0 E_0}{(1+\nu)(2-\nu)} \cdot \sqrt{g(t)}, \quad (17)$$

$$K_m(t) = \frac{16}{3}a(t)^3 S(t) = \frac{8a_0^3 E_0}{3(1+\nu)} \cdot \frac{1}{\sqrt{g(t)}}. \quad (18)$$

In addition, consider the case where only normal force is applied. Although no tangential or torsional load is present, the initial values of tangential stiffness and torsional stiffness still vary over time, expressed as follows:

$$K_{\tau,0}(t) = \frac{4a(t)S(0)}{2-\nu} = \frac{2a_0 E_0}{(1+\nu)(2-\nu)} \cdot \frac{1}{\sqrt{g(t)}}, \quad (19)$$

$$K_{m,0}(t) = \frac{16}{3}a(t)^3 S(0) = \frac{8a_0^3}{3(1+\nu)} \cdot \left[\frac{1}{g(t)} \right]^{\frac{3}{2}}. \quad (20)$$

Eqs. (16)–(18) describe the effect of loading on stiffness in the same direction. In contrast, Eqs. (19) and (20) illustrate the stiffness enhancement during the normal contact process [22]

(assuming that the normal contact has already reached a steady state): After applying a step normal force, the contact area increases with the normal indentation, and the contact force distribution becomes more uniform. As a result, the resistance to tangential loads is strengthened.

According to [7], common soft fingertip contact is considered: it can transmit contact forces along three axes and deliver a contact torque about the inward normal of the tangential contact surface. Introducing the contact stiffness matrix in the local coordinate system:

$$\mathbf{K}_j(t) = \mathbf{J}^T \cdot \text{diag}([K_n(t), K_\tau(t), K_m(t)]) \cdot \mathbf{J}, \quad (21)$$

$$\text{where } \mathbf{J} = \begin{bmatrix} 0 & 0 & 1 & 0 & 0 & 0 \\ 1 & 0 & 0 & 0 & 0 & 0 \\ 0 & 0 & 0 & 0 & 0 & 1 \end{bmatrix}, \quad (22)$$

\mathbf{J} represents the Jacobian matrix.

In Eq. (21), \mathbf{K}_j represents the instantaneous stiffness matrix of fingertip j , quantitatively describing the static mechanical properties of a single contact surface. In this article, normal force, tangential force, and normal torque are considered, while bending impedance along the x and y axes is neglected. As a result, the rank of \mathbf{K}_j is 3. Besides, if other contact models are considered (such as line contact or point contact models), the stiffness for contact forces or torques along or about the corresponding axes can be set to zero. For the 6-d limit surface model, a full-rank stiffness matrix is required to reflect that both 3-d forces and 3-d torques can be transmitted through the patch contact interface.

C. Grasp Evaluation Metrics

A 2-d grasping framework is established with multiple fingertips contacting the object, as shown in Fig. 1(d). Suppose there are N fingertips in total, with the local coordinate system of the j -th fingertip denoted as $\{O_j\}$, the gripper coordinate system as $\{O\}$, and the object's center of mass as C . The coordinate transformation matrix from $\{O_j\}$ to $\{O\}$ is denoted as

$$\mathbf{T}_j = \begin{bmatrix} \mathbf{R}_j & \mathbf{t}_j \\ 0 & 1 \end{bmatrix}, \quad (23)$$

where \mathbf{R}_j is the rotation matrix and \mathbf{t}_j is the translation vector. Following [7], the adjoint transformation matrix can be defined based on \mathbf{T}_j to describe the coordinate transformation as follows:

$$\mathbf{A}_j = \begin{bmatrix} \mathbf{R}_j & 0 \\ \mathbf{t}_j \mathbf{R}_j & \mathbf{R}_j \end{bmatrix}. \quad (24)$$

Assuming the object is subjected to a virtual wrench increment $\delta \mathbf{w}$, and the corresponding virtual small displacements $\delta \xi$. We transform the single-finger stiffness matrices into the gripper coordinate system $\{O\}$ to obtain the instantaneous force-displacement characteristics:

$$\delta \mathbf{w} = \mathbf{K} \cdot \delta \xi, \quad (25)$$

$$\mathbf{K}(t) = \sum_{j=1}^N (\mathbf{A}_j)^{-T} \cdot \mathbf{K}_j(t) \cdot (\mathbf{A}_j)^{-1}, \quad (26)$$

\mathbf{K} describes the overall compliance model of the grasp at the current moment, and its size depends on the number of fingers and the dimensionality of the wrench. During the grasping process, the grasp stiffness matrix evolves dynamically. If a constant step grasp force is applied from the initial time, the variation of \mathbf{K} is governed by Eqs. (16)–(20). Although the grasp stiffness matrix itself cannot be directly used as a grasp quality metric, it is possible to achieve the evaluation of grasp quality by linking certain eigenvalues or states contained in the dynamic mapping to grasp performance.

Inspired by related studies [35], [36], this article constructs a grasp quality metric based on the singular values of the stiffness matrix. Each singular value quantifies the stiffness of the current grasp in a specific direction, with higher singular values indicating stronger impedance transmission capability in that direction. Therefore, the first grasp quality metric is defined as the geometric mean of the singular values in the stiffness matrix $\mathbf{K}(t)$:

$$G_1(t) = \sqrt[n]{\prod_{i=1}^n \sigma_i(t)}, \quad (27)$$

where n denotes the number of singular values. G_1 accounts for singular values in all directions, reflecting the global contact stiffness. A larger G_1 indicates higher overall stability and impedance of the current grasp configuration.

Considering that object detachment typically occurs along the direction with the lowest impedance, we further introduce the minimum singular value in the stiffness matrix to reflect the lower bound of stability:

$$G_2(t) = \sqrt{\sigma_{min}^F(t) \cdot \sigma_{min}^M(t)}. \quad (28)$$

Here, σ_{min}^F denotes the minimum singular value corresponding to the force components, and σ_{min}^M corresponds to the torque components. According to [35], as G_2 approaches zero, the grasp offers less resistance in the direction with the lowest impedance. Therefore, a good grasp configuration should exhibit higher values of both G_1 and G_2 .

Finally, the equilibrium of grasping in terms of force and torque components is considered. This metric is defined as the ratio between the singular values corresponding to the force components and that of the torque components in $\mathbf{K}(t)$:

$$G_3(t) = \frac{\sqrt[n^F]{\prod_{i=1}^{n^F} \sigma_i^F(t)}}{\sqrt[n^M]{\prod_{i=1}^{n^M} \sigma_i(t)}}, \quad (29)$$

where n^F and n^M represent the number of singular values corresponding to the force and torque components. A larger G_3 indicates that the current contact state is more biased toward tangential impedance, whereas a smaller value implies a higher proportion of torsional impedance.

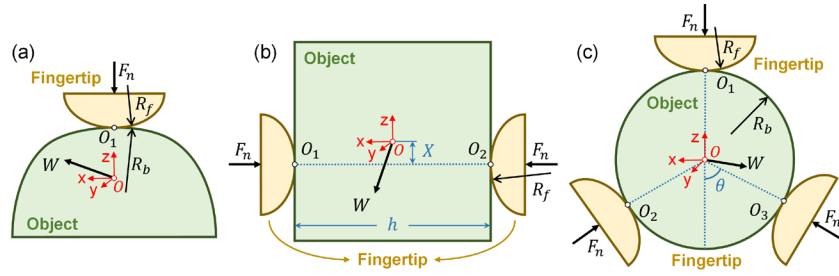


Fig. 3. Case analysis. (a) Single-finger contact. (b) Two-finger grasping. (c) Three-finger grasping.

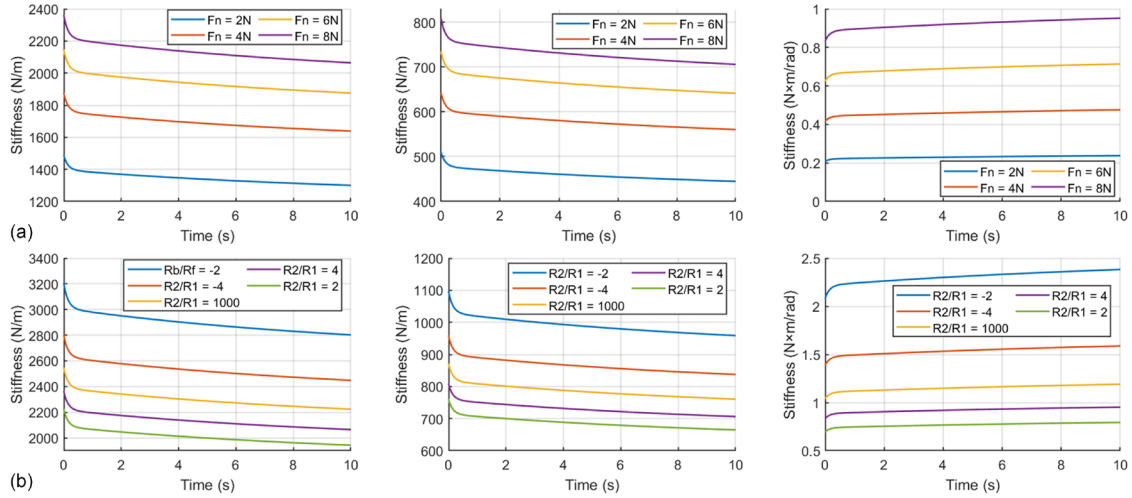


Fig. 4. Time evolution of contact stiffness under tangential and torsional loads. (a) Comparison of different normal forces. (b) Comparison of different contact local curvatures.

Using these three dynamic metrics together, we can obtain a comprehensive understanding of grasping performance during viscoelastic contact. Unlike other evaluation tasks, the dynamic nature of these metrics stems from the creep characteristics inherent in viscoelastic contact. Therefore, even though the model reflects a fixed grasp configuration (i.e., with constant geometric transformations), the use of viscoelastic fingertips causes the grasp quality to vary throughout the contact process.

III. SIMULATED CASE ANALYSIS

This section analyzes the influence of viscoelastic contact on different grasp configurations through three case studies, as shown in Fig. 3. Simulations are conducted in MATLAB using the VHB 4910 material parameters described in Section II. The fingertip contact surface is modeled as an arc with a radius of $R_f = 100\text{mm}$. Unless otherwise specified, the object's contact surface is assumed to be flat.

A. Case 1: Single finger

In Fig. 3(a), we analyze the contact stiffness of a single fingertip. First, the time-varying behavior of contact stiffness under tangential and torsional loads is examined, as described in Eqs. (16)–(18). The results in Fig. 4 show that, with increasing load application time, the normal stiffness K_n and tangential stiffness K_t gradually decrease. However, the rate

of decrease slows over time, and eventually reach a steady state. This indicates a characteristic of initial reduction

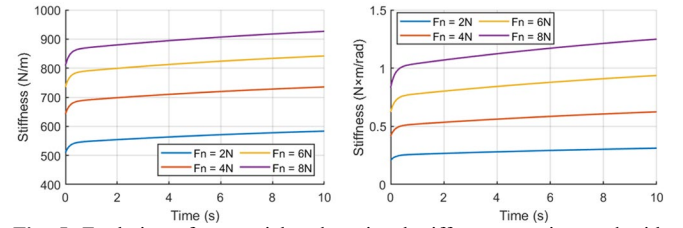


Fig. 5. Evolution of tangential and torsional stiffness over time and with varying normal force under normal loading only.

followed by stabilization. In contrast, the torsional stiffness K_m exhibits an increasing trend, mainly due to the expansion of the contact area.

Fig. 4(a) and 4(b) illustrate the influence of normal force and contact curvature on stiffness, respectively. The radii of the fingertip and the object are denoted as R_f and R_b , where $R_b > 0$ indicates a convex surface and $R_b < 0$ indicates a concave one. When the object is flat, R_b tends to infinity (approximated as 1000 times R_f). For fixed material properties and contact curvature, all three stiffness coefficients increase with greater normal force. Moreover, based on Eqs. (14)–(18), K_n and K_t exhibit diminishing growth rates with

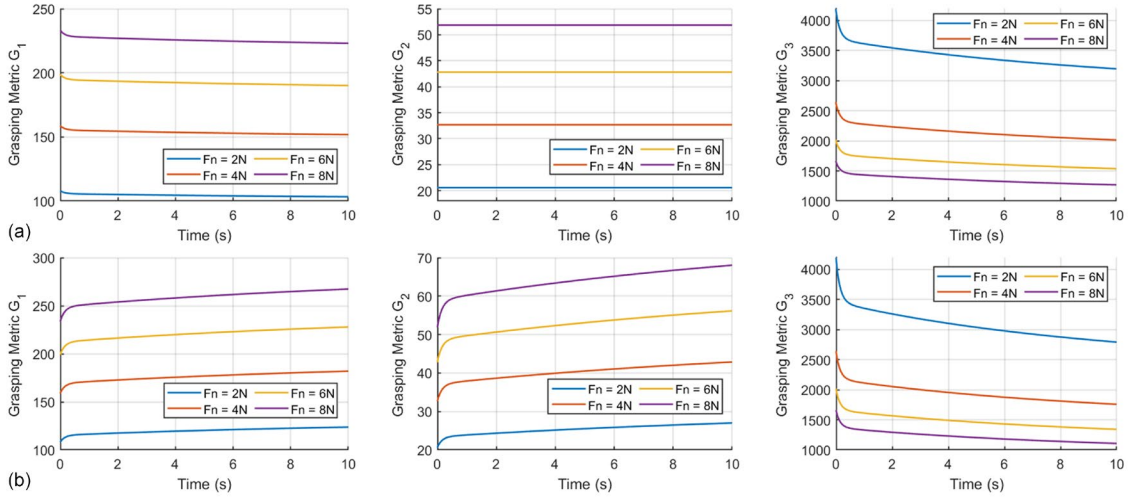


Fig. 6. Time Evolution of grasping metrics under two-finger grasping with different normal forces. (a) With tangential and torsional loads. (b) With normal load only.

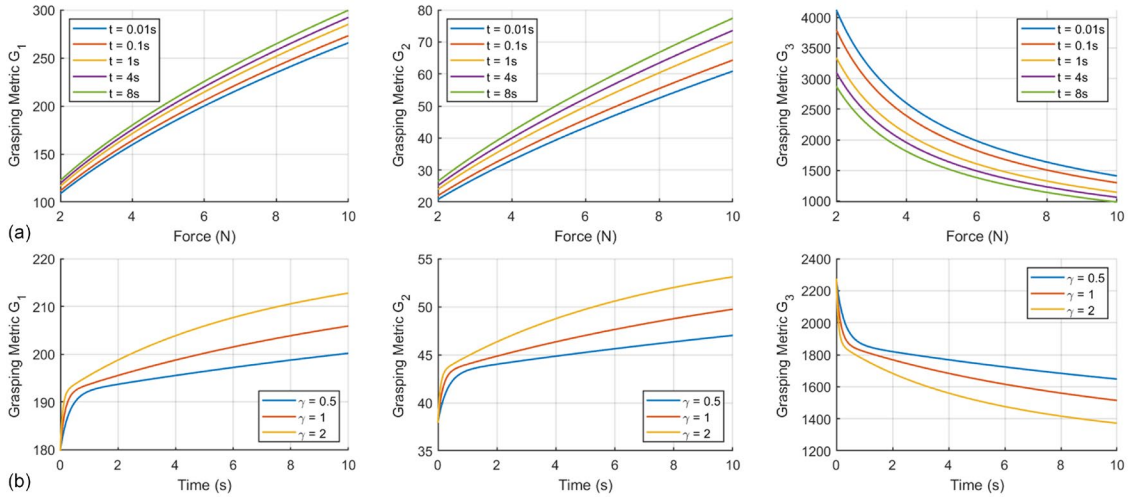


Fig. 7. Influence of normal force and viscosity on grasp quality under two-finger grasp. (a) Effect of varying normal forces on the grasping metrics. (b) Comparison of grasping metrics under different viscosity levels in the two-finger grasp configuration.

increasing normal force, while K_m increases linearly. Regarding contact curvature, contact between a fingertip and an object with a negative radius ratio leads to higher stiffness coefficients than contact with a positive radius ratio. This aligns with intuition, as more enveloping contact geometries provide greater stability.

Fig. 5 illustrates the behavior described in Eqs. (16), (19), and (20), namely, the time-dependent stiffness variation resulting from the change in contact area under constant normal force. As the duration of the applied load increases, both tangential and torsional stiffness increase despite the absence of external forces in the tangential direction. Furthermore, the trend of stiffness variation with respect to normal force is consistent with the case where a step tangential load is applied before the normal response has stabilized. Therefore, when considering viscoelastic contact characteristics, normal contact alone can induce changes in the

in-plane stiffness, which specifically increases with either longer contact duration or greater normal force.

B. Case 2: Two fingers

Consider the two-finger grasping configuration shown in Fig. 3(b), where two fingertips make parallel contact with the object, and the object's contact surface is flat. The variable X represents the offset of the contact position along the Z -axis. Based on the previously derived contact stiffness coefficients, the contact stiffness matrices are transformed into the global grasping stiffness matrix using the adjoint coordinate transformation. Then, the three grasp quality metrics defined in Eqs. (27)–(29) are constructed and analyzed accordingly.

Fig. 6 illustrates the time-varying behavior of the grasping metrics. Overall, larger normal forces result in higher values of G_1 and G_2 , and a lower value of G_3 . When both tangential and torsional loads are present, G_1 and G_2 remain nearly

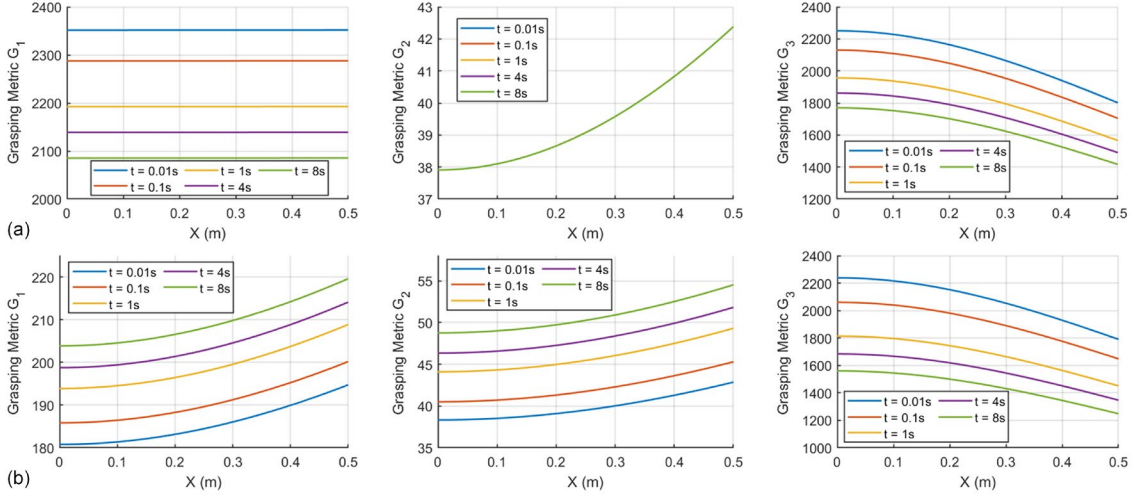


Fig. 8. Grasping metrics vary with the offset distance X at different times under two-finger grasp. The normal force is set to 5 N. (a) With tangential and torsional loads. (b) With normal force only.

constant with increasing creep time, while G_3 gradually decreases [see Fig. 6(a)]. This indicates that both the overall contact impedance and the impedance in the weakest direction remain unchanged, whereas the stability in the dominant direction improves. In contrast, when only the normal force is applied, both G_1 and G_2 increase with time, as shown in Fig. 6(b). Therefore, when only normal force is applied, grasp quality improves as the application time increases, with an increasing emphasis on tangential impedance.

The effects of normal force and viscosity on grasp quality are further examined. As shown in Fig. 7(a), under normal loading only, the three grasping metrics are evaluated with respect to varying normal forces at specific times. Both G_1 and G_2 increase almost linearly with the normal force, while G_3 decreases gradually, with a more pronounced nonlinear trend. Fig. 7(b) compares the effect of viscosity using the settings described in Table I and Fig. 2. The results show that the evolution of G_3 closely resembles the inverse of the function $g_y(t)$, whereas the evolution of G_1 and G_2 are similar to that of $g_y(t)$. Therefore, a higher viscosity means a greater effect on enhancing grasping quality.

As shown in Fig. 8, the grasping metrics are compared under different configurations by varying the value of X . Fig. 8(a) analyzes the effect of displacement offset under both tangential and torsional loads. For the two-finger contact case in the 2-d model, G_2 increases with the offset distance, while G_3 decreases. Meanwhile, G_1 remains independent. This indicates that the variation in grasp configuration primarily affects torsional stiffness rather than tangential stiffness. Moreover, considering that G_1 depends only on the normal force and viscosity, and G_2 is independent of the loading time, both can serve as reliable indicators of grasp configuration or contact parameters under such conditions.

In the case where only normal force is applied [see Fig. 8(b)], the metrics exhibit the same trend. The difference lies in that G_1 also increases with time, and both G_1 and G_2 grow

larger with longer loading durations. As the variation rates of the three metrics with respect to X remain consistent over time, the relative impedance among different initial grasp configurations remains approximately constant during the creep.

C. Case 3: Three fingers

Fig. 3(b) analyzes a typical scenario of three-finger grasping of a spherical object to investigate the influence of viscoelastic properties on an ideal grasp configuration. The grasp configuration is adjusted by changing the angles of the three fingertips relative to the object's center. Fingertip 1 is fixed in position, while fingertips 2 and 3 are placed symmetrically. The coordinate transformations are defined as follows:

$$\mathbf{R}_i = \begin{cases} R_y\left(\frac{\pi}{2}\right), & i = 1 \\ R_y\left(\frac{3\pi}{2} - \theta\right), & i = 2, \\ R_y\left(\frac{3\pi}{2} + \theta\right), & i = 3 \end{cases} \quad (29)$$

$$\text{where } R_y(\varphi) = \begin{bmatrix} \cos(\varphi) & 0 & \sin \varphi \\ 0 & 0 & 0 \\ -\sin \varphi & 0 & \cos(\varphi) \end{bmatrix}. \quad (30)$$

By varying the offset angle θ , the rotational symmetry of the grasp configuration can be altered. Empirically, a symmetric grasp with three contact points evenly distributed along the great circle of a spherical object (i.e., $\theta = \pi/3$) is considered the optimal configuration. We aim to verify whether the defined grasping metrics reach their maximum values under this condition and whether the viscoelastic effect influences the position of the optimal configuration.

As shown in Fig. 9, the grasping metrics are evaluated with respect to θ at five selected time points. The results indicate that G_1 , G_2 , and G_3 exhibit similar time-dependent behaviors

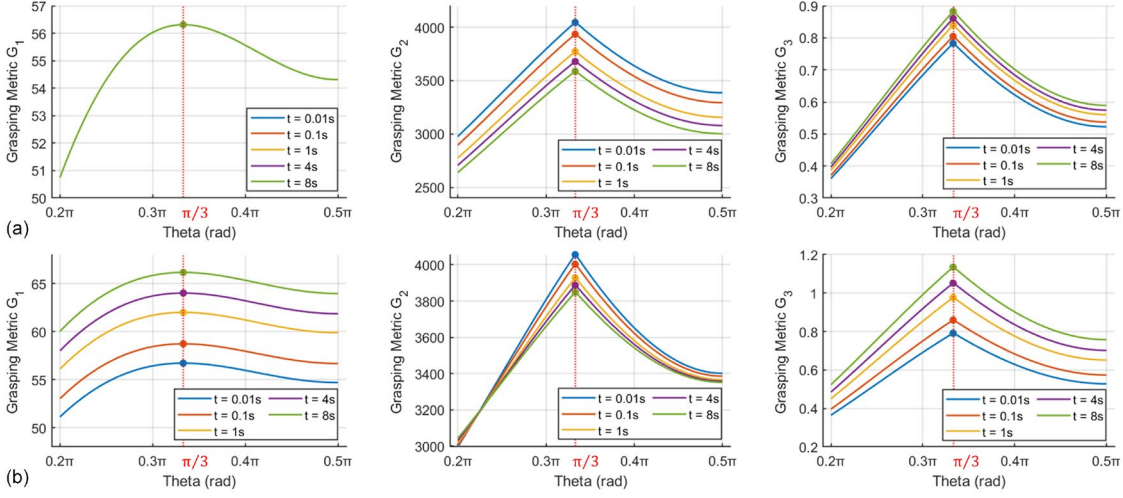


Fig. 9. The grasping metrics of three-finger grasping as a function of the offset angle θ at different times. The normal force is set to 5N. (a) With tangential and torsional loads. (b) With normal load only.

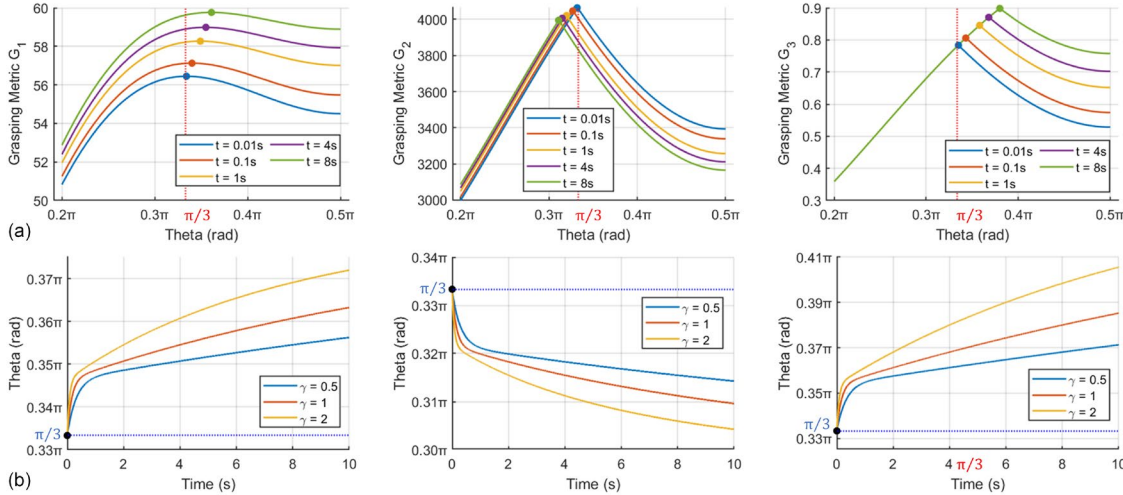


Fig. 10. Viscoelastic effects cause an offset angle in the optimal grasping configuration from the initial value under a normal force of 5 N. (a) Variation of grasping metrics with the offset angle θ at different times when only one fingertip is viscoelastic. (b) Influence of different viscosities on the optimal offset angle θ corresponding to the ideal grasping configuration.

as in the case shown in Fig. 6, and all reach their maximum values at $\theta = \pi/3$, which confirms the validity of the proposed metrics. The difference between the two cases lies in the fact that, under tangential and torsional loading, G_1 remains unaffected by time, similar to the two-finger grasping scenario. Moreover, the variation in G_1 reflects the influence of grasp configuration on the stiffness enhancement process: when θ is too small or too large, the lower bound of stability shows little variation over time, whereas it increases more significantly when θ approaches $\pi/3$.

Consider the case where fingertip 1 exhibits viscoelasticity, while fingertips 2 and 3 are purely elastic with a modulus of E_0 . Fig. 10(a) compares the variations of G_1 , G_2 , and G_3 with respect to the offset angle θ . When there is a viscosity mismatch, the optimal grasp configuration shifts over time: initially, all three grasping metrics reach their maximum at

$\theta = \pi/3$. As creep progresses, the configurations corresponding to the maximum values of G_1 and G_3 shift in the positive direction along the horizontal axis, while that of G_2 shifts in the opposite direction. This indicates that different aspects of grasp quality evolve differently: when fingertips 2 and 3 move closer to fingertip 1, the overall grasp quality improves and becomes more biased toward the tangential components, while the stability in the low-impedance direction decreases.

The effect of varying the viscosity of fingertip 1 is further examined in Fig. 10(b). The results show that before approximately 0.2 seconds, the shift in the optimal grasp configuration occurs more rapidly. A higher viscosity leads to a faster change and a greater deviation of the optimal grasp configuration from $\theta = \pi/3$ at any given time. These findings indicate that the influence of viscoelasticity on the

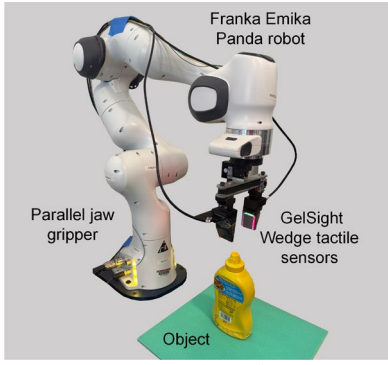


Fig. 11. Experimental setup.

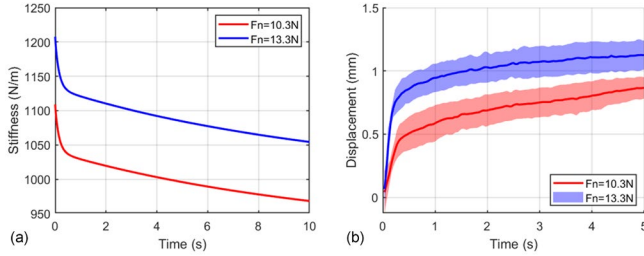


Fig. 12. Comparison of tangential stiffness under different normal forces with tangential loading applied. (a) Theoretical results of tangential stiffness. (b) Experimental results of object tangential displacement under different conditions.

optimal grasp configuration becomes more significant as the viscosity increases.

IV. EXPERIMENTAL CASE ANALYSIS

A. Experimental Setup

This section presents the validation of the proposed method through real-world experiments. As shown in Fig. 11, two vision-based tactile sensors, GelSight Wedge [37], were selected to provide feedback on contact geometry, and were integrated into a custom-designed two-finger parallel gripper [38]. A mustard bottle was chosen as the grasping object due to its symmetric structure and easily recognizable tactile contour. In the experiment, the gripper applied a constant grasp force, while a robotic arm performs the object-lifting motion. Thus, this setup satisfies the creep behavior modeled in Section II. The tactile sensors convert contact deformation into tactile images, enabling the measurement of in-hand creep displacement through contour detection and optical flow analysis. Finally, features such as creep stiffness and grasping metrics are compared to evaluate different configurations.

B. Evaluation of Viscoelastic Effects

In the first part of the experiment, the gripper grasped the object with different normal forces ($F_n = 10.3N$ and $F_n = 13.3N$), while other conditions, such as preload time and grasping position, were kept constant. According to Section II, the tangential creep stiffness of the fingertips gradually decreased from an initially high value due to viscoelasticity, as shown in Fig. 12(a). Thus, the in-hand creep displacement of

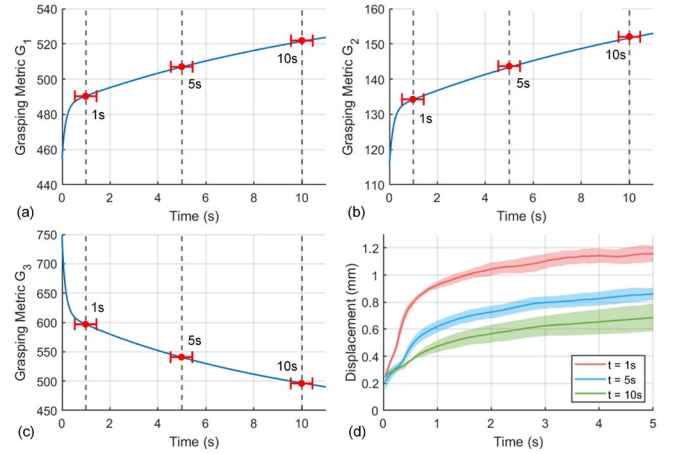


Fig. 13. Effect of different preload durations on grasp enhancement under normal loading only. (a)–(c) Theoretical results of grasping metrics over time. (d) Experimental results of object tangential displacement under different conditions.

the object gradually increased, with a decreasing growth rate. Fig. 12(b) shows the total measured tangential displacement of the object for the two cases. Each grasp was repeated five times, and the average displacement was computed. Although the measured displacement was not exactly equal to the creep displacement due to the presence of slip and overall pad motion, it was approximately proportional. The results showed that the evolution of tangential displacement aligned with the variation in tangential stiffness. Moreover, it was observed that a higher normal force resulted in a greater tangential stiffness. Accordingly, the corresponding displacement was also larger, which met experimental expectations.

The stiffness enhancement during viscoelastic contact was further investigated. First, the object was grasped with a constant force $F_n = 13.3N$ for a predetermined period before being lifted. Three different preload durations were selected to compare the corresponding tangential displacements. The grasp quality metrics were computed based on the theoretical analysis in Section II, as shown in Fig. 13(a)–(c). As the preload time increased, both the overall impedance and the minimum impedance increased. Meanwhile, the grasp quality shifted toward the tangential direction, which means that tangential stability improved with longer preload durations. The experimental results are presented in Fig. 13(d). The outcomes demonstrated consistency between theory and experiment: the longer the preload time, the greater the tangential impedance, resulting in smaller and more gradually increasing tangential displacements.

C. Comparison of Grasping Configurations

Considering the specific design and shape of the grasped object, two grasping conditions were proposed to ensure complete contact between the fingers and the object, as shown in Fig. 14(a). For the two configurations, aside from differences in the load transmission matrix, config 1 involved only tangential loading, while config 2 involved both

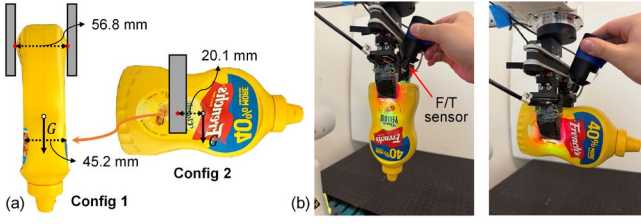


Fig. 14. (a) Two grasp configurations. (b) Initialization of experiments.

tangential and torsional loading. Inspired by the “grasp perturbation test” in [36], the experiment was designed as follows: a constant normal force was applied for a sufficiently long duration t_1 (allowing the normal contact to reach stability), after which the object was lifted. After an additional period t_2 , a downward force was rapidly applied through a handle and conical indenter aligned vertically with the object’s center of mass, until the object dropped. A force sensor mounted behind the indenter recorded the peak applied normal force ΔF , as illustrated in Fig. 14(b). By comparing the required ΔF to cause the object to fall, the stability of different grasp configurations under varying t_2 values were evaluated. In this context, since t_2 was sufficiently long, the normal impedance and contact area reached a steady state. During the period from t_1 to $t_1 + t_2$, the directional stiffness in each axis could be calculated as:

$$K_n = \frac{2a(\infty)E(\infty)}{1 - \nu^2} = \frac{2a_0E_0}{1 - \nu^2} \cdot \sqrt{g(\infty)}, \quad (32)$$

$$K_\tau = \frac{4a(\infty)S(t)}{2 - \nu} = \frac{2a_0E_0}{(1 + \nu)(2 - \nu)} \cdot \frac{g(t)}{\sqrt{g(\infty)}}, \quad (33)$$

$$K_m = \begin{cases} \frac{16}{3}a(\infty)^3S(t) = \\ \frac{8a_0^3}{3(1 + \nu)} \cdot \frac{g(t)}{[g(\infty)]^{\frac{3}{2}}}, & \text{for config 1} \\ \frac{16}{3}a(\infty)^3S(0) = \\ \frac{8a_0^3}{3(1 + \nu)} \cdot \frac{1}{[g(\infty)]^{\frac{3}{2}}}, & \text{for config 2} \end{cases}. \quad (34)$$

For the two grasp configurations, two tangential loading times, $t_2 = 1s$ and $t_2 = 5s$, were selected, resulting in four different cases. The experimental results are shown in Fig. 15. It was observed that compared to config 1, config 2 had smaller values of G_1 and G_2 , but a larger value of G_3 . The former indicates that config 2 has lower overall stability and a lower stability lower bound, while the latter implies a higher proportion of tangential impedance. Therefore, config 2 is more likely to fail due to torque effects. Additionally, the variation of grasping metrics over time shows that stability gradually decreases. In summary, the grasp quality ranking is judged as:

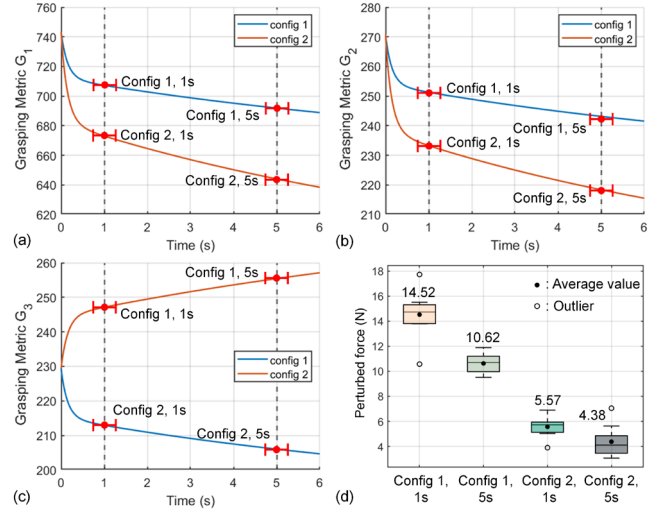


Fig. 15. Comparison of stability between different grasp configurations. (a) Theoretical results of grasping metrics varying with time under different conditions. (b) Comparison of maximum perturbation forces under different conditions.

$$\begin{aligned} (\text{Config 1, 1s}) &> (\text{Config 1, 5s}) > \\ (\text{Config 2, 1s}) &> (\text{Config 2, 5s}). \end{aligned} \quad (35)$$

The experimental results shown in Fig. 15(d) validate the expected stability ranking: a grasp configuration that can resist a larger external wrench before failure corresponds to better in-hand object stability. Overall, the experimental findings align with the predictions of the grasp quality curves, and demonstrate the effectiveness of the proposed evaluation method.

V. DISCUSSION

Simulation and experimental results show that fingertip viscoelasticity affects grasp impedance and stability in three main aspects:

- 1) Tangential and torsional stiffness gradually decrease under applied load. When tangential forces or torques exist at the contact surface, the corresponding creep displacement increases over time, causing a decline in related grasping metrics. This indicates that the fingertip’s grasp quality is highest initially but rapidly decreases as the load duration increases. Thus, under low-frequency varying loads, the fingertip gradually transitions from a high-strength, high-frequency instantaneous modulus to a lower-strength, low-frequency equilibrium modulus.
- 2) The changes of contact geometry under normal loading can lead to stiffness enhancement. When only normal forces are applied, the contact area expands, causing the initial tangential and torsional stiffness as well as grasp metrics to increase and stabilize. Therefore, longer preload durations correspond to greater improvements in initial contact stability.
- 3) The optimal grasp configuration shifts over time. For a given scenario, different grasp configurations may exhibit different grasp qualities. The time-dependent

viscoelasticity affects the grasp metrics of each configuration and may cause the optimal grasp configuration (with the highest grasp quality) to shift at any given time.

Based on these insights, this article proposes a strategy to enhance grasping performance by leveraging viscoelastic contact characteristics:

- 1) Leveraging time-dependent stiffness variations to improve resistance to high-frequency external disturbances. For objects subjected to rapidly changing loads over time (e.g., electric mixers and toothbrushes), the viscous component of the fingertip can maintain a high-frequency stiffness model, thereby providing greater effective contact quality.
- 2) Utilizing stiffness enhancement to improve grasp stability. By applying a sufficiently long preload force before grasping the object, the contact forces become more uniformly distributed and the contact area maximized. Under this condition, even with the same grasp force, the contact surface can offer greater tangential and torsional impedance.
- 3) Actively adjusting grasp configurations to adapt to temporal characteristics. Since the ideal grasp candidate may change over time due to viscoelastic effects, selecting a configuration with higher grasp quality at specific times or dynamically adjusting the grasp synthesis can help maintain an optimal grasp throughout the interaction.

VI. CONCLUSION

This article proposes a grasping model and evaluation method that consider the viscoelastic properties of materials to assess the impact of viscoelastic contact on grasping. Considering the creep phenomena commonly observed during grasping tasks, a generalized grasp stiffness matrix is constructed using the generalized Kelvin or Maxwell models. Three grasp evaluation metrics are introduced to characterize the time-dependent variations in grasp quality caused by viscoelasticity. Simulation analyses and robotic experiments are conducted to demonstrate the application of the proposed method in evaluating different grasping scenarios and to verify its effectiveness. The main contributions of this work are further summarized as three key strategies for improving grasping performance by incorporating viscoelastic contact characteristics.

The proposed analytical method can be used for impedance and grasp quality analysis of grasping interfaces involving viscoelastic contact. Other types of grasp quality metrics and calculation methods can also be integrated into this framework to accommodate various contact conditions (e.g., relaxation phenomena under active displacement control). Future work will further introduce friction-limit-based evaluation metrics to enhance the completeness of grasp quality assessment, and explore the practical application of the evaluation framework.

REFERENCES

- [1] A. Billard and D. Kragic, "Trends and challenges in robot manipulation," *Science*, vol. 364, no. 6446, 2019, Art. no. eaat8414.
- [2] B. H. Zhang, Y. X. Xie, J. Zhou, K. Wang, and Z. Zhang, "State-of-the-art robotic grippers, grasping and control strategies, as well as their applications in agricultural robots: A review," *Comput. Electron. Agric.*, vol. 177, 2020, Art. no. 105694.
- [3] Y. Laili, Z. Chen, L. Ren, X. Wang, and M. J. Deen, "Custom grasping: A region-based robotic grasping detection method in industrial cyber-physical systems," *IEEE Trans. Automat. Sci. Eng.*, vol. 20, no. 1, pp. 88-100, Jan. 2023.
- [4] T. Li et al., "A comprehensive review of robot intelligent grasping based on tactile perception," *Robot. Comput.-Integr. Manuf.*, vol. 90, 2024, Art. no. 102792.
- [5] A. Rodriguez, "The unstable queen: Uncertainty, mechanics, and tactile feedback," *Sci. Robot.*, vol. 6, no. 54, pp. 1-2, 2021.
- [6] G. Liu, J. Xu, X. Wang, and Z. Li, "On quality functions for grasp synthesis, fixture planning, and coordinated manipulation," *IEEE Trans. Automat. Sci. Eng.*, vol. 1, no. 2, pp. 146-162, 2004.
- [7] H. Dong, C. Qiu, D. K. Prasad, Y. Pan, J. Dai, and I.-M. Chen, "Enabling grasp action: Generalized quality evaluation of grasp stability via contact stiffness from contact mechanics insight," *Mechanism Mach. Theory*, vol. 134, pp. 625-644, 2019.
- [8] M. Li, L. Zhang, T. Li, and Y. Jiang, "Learning gentle grasping from human-free force control demonstration," *IEEE Robot. Autom. Lett.*, vol. 10, no. 3, pp. 2391-2398, Mar. 2025.
- [9] M. A. Roa and R. Suárez, "Grasp quality measures: review and performance," *Auto. Robot.*, vol. 38, pp. 65-88, 2015.
- [10] H. Mnyussiwalla, P. Seguin, P. Vulliez, and J.-P. Gazeau, "Evaluation and selection of grasp quality criteria for dexterous manipulation," *J. Intell. Robot. Syst.*, vol. 104, no. 2, p. 20, 2022.
- [11] E. Rimon, J. W. Burdick, and T. Omata, "A polyhedral bound on the indeterminate contact forces in planar quasi-rigid fixturing and grasping arrangements," *IEEE Trans. Robot.*, vol. 22, no. 2, pp. 240-255, 2006.
- [12] E. Rimon, R. Mason, J. W. Burdick, and Y. Or, "A general stance stability test based on stratified morse theory with application to quasi-static locomotion planning," *IEEE Trans. Robot.*, vol. 24, no. 3, pp. 626-641, 2008.
- [13] M. Pozzi, A. Sundaram, M. Malvezzi, D. Prattichizzo, and M. A. Roa, "Grasp quality evaluation in underactuated robotic hands," in *Proc. 2016 IEEE/RSJ Int. Conf. Intell. Robots Syst. (IROS)*, Oct. 2016, pp. 1946-1953.
- [14] T. N. Le, J. Lundell, F. J. Abu-Dakka, and V. Kyrki, "A novel simulation-based quality metric for evaluating grasps on 3D deformable objects," In *Proc. 2023 IEEE/RSJ Int. Conf. Intell. Robots Syst. (IROS)*, Oct. 2023, pp. 3123-3129.

- [15] T. Yamada, T. Taki, M. Yamada, Y. Funahashi, and H. Yamamoto, "Static stability analysis of spatial grasps including contact surface geometry," *Adv. Robot.*, vol. 25, no. 3/4, pp. 447–472, 2011.
- [16] C. Rubert, B. León, A. Morales, and J. Sancho-Bru, "Characterisation of grasp quality metrics," *J. Intell. Robot. Syst.*, vol. 89, nos. 3–4, pp. 319–342, 2018.
- [17] S. Zaidi, M. Maselli, C. Laschi, and M. Cianchetti, "Actuation technologies for soft robot grippers and manipulators: A review," *Curr. Robot. Rep.*, vol. 2, no. 3, pp. 355–369, 2021.
- [18] N. Elango and A. Faudzi, "A review article: Investigations on soft materials for soft robot manipulations," *Int. J. Adv. Manuf. Technol.*, vol. 80, nos. 5–8, pp. 1027–1037, 2015.
- [19] M. Li, L. Zhang, Y. H. Zhou, T. Li, and Y. Jiang, "EasyCalib: Simple and low-cost in-situ calibration for force reconstruction with vision-based tactile sensors," *IEEE Robot. Automat. Lett.*, vol. 9, no. 9, pp. 7803–7810, Sep. 2024.
- [20] P. Tiezzi and I. Kao, "Modeling of viscoelastic contacts and evolution of limit surface for robotic contact interface," *IEEE Trans. Robot.*, vol. 23, no. 2, pp. 206–217, 2007.
- [21] C.-H.-D. Tsai, I. Kao, M. Higashimori, and M. Kaneko, "Modeling, sensing, and interpretation of viscoelastic contact interface," *Adv. Robot.*, vol. 26, nos. 11–12, pp. 1393–1418, 2012.
- [22] J. Armendariz, F. Machorro-Fernandez, V. Parra-Vega, R. Garcia Rodriguez, and S. Hirai, "Improving physical human-robot interaction through viscoelastic soft fingertips," in 2012 *Proc. IEEE/RSJ Int. Conf. Intell. Robots Syst. (IROS)*, Oct. 2012, pp. 2977–2984.
- [23] C. D. Tsai, I. Kao, K. Yoshimoto, M. Higashimori, and M. Kaneko, "An experimental study and modeling of loading and unloading of nonlinear viscoelastic contacts," in *Proc. 2009 IEEE/RSJ Int. Conf. Intell. Robots Syst. (IROS)*, Oct. 2009, pp. 3737–3743.
- [24] C. D. Tsai, J. Nishiyama, I. Kao, M. Higashimori and M. Kaneko, "Study of the relationship between the strain and strain rate for viscoelastic contact interface in robotic grasping," in *Proc. 2010 IEEE/RSJ Int. Conf. Intell. Robots Syst. (IROS)*, Oct. 2010, pp. 592–597.
- [25] Q. Li et al., "Contact force/torque control based on viscoelastic model for stable bipedal walking on indefinite uneven terrain," *IEEE Trans. Automat. Sci. Eng.*, vol. 16, no. 4, pp. 1627–1639, Oct. 2019.
- [26] S. Ding, Y. Hu, B. Jian, Y. Zhang, R. Xia, and G. Hu, "A review and comparative analysis of normal contact force models for viscoelastic particles," *Int. J. Impact Eng.*, vol. 189, p. 104968, 2024.
- [27] Q. Lin, J. W. Burdick, and E. Rimon, "A stiffness-based quality measure for compliant grasps and fixtures," *IEEE Trans. Robot. Automat.*, vol. 16, pp. 675–688, Dec. 2000.
- [28] C. J. Stabile, D. J. Levine, G. M. Iyer, C. Majidi, and K. T. Turner, "The role of stiffness in versatile robotic grasping," *IEEE Robot. Automat. Lett.*, vol. 7, no. 2, pp. 4733–4740, 2022.
- [29] W. N. Findley, J. S. Lai, and K. Onaran, *Creep and relaxation of nonlinear viscoelastic materials*. Amsterdam, The Netherlands: North-Holland, 1976.
- [30] M. A. Meyers and K. K. Chawla, *Mechanical Behavior of Materials*, Cambridge, U.K.: Cambridge Univ. Press, 2008.
- [31] M. Hossain, D. K. Vu, and P. Steinmann, "Experimental study and numerical modelling of VHB 4910 polymer," *Comput. Mater. Sci.*, vol. 59, pp. 65–74, 2012.
- [32] X. Huang, X. Feng, and B. Chen, "Equivalences of the generalized viscoelastic models and their inherent properties," *Chin J. Theor. Appl. Mech.*, vol. 42, no. 1, pp. 65–73, 2010.
- [33] J. H. Kim, D. Yang, and S. Park, "Experimental validation for the interconversion between generalized Kelvin–Voigt and Maxwell models using human skin tissues," *J. Biomech.*, vol. 162, p. 111908, Dec. 2023.
- [34] V. L. Popov, *Contact mechanics and friction*. Berlin, Springer Berlin Heidelberg, 2010.
- [35] B.-H. Kim, S.-R. Oh, B.-J. Yi, and I. H. Suh, "Optimal grasping based on non-dimensionalized performance indices," in *Proc. IEEE/RSJ Int. Conf. Intell. Robots Syst. (IROS)*, Maui, HI, USA, 2001, pp. 949–956.
- [36] P. Song, J. A. C. Ramon, and Y. Mezouar, "Dynamic evaluation of deformable object grasping," *IEEE Robot. Automat. Lett.*, vol. 7, no. 2, pp. 4392–4399, 2022.
- [37] S. Wang, Y. She, B. Romero and E. Adelson, "GelSight wedge: measuring high-resolution 3-d contact geometry with a compact robot finger," in *Proc. 2021 IEEE Int. Conf. Robot. Automat. (ICRA)*, May 2021, pp. 6468–6475.
- [38] J. Zhao, Y. Ma, and E. H. Adelson, "Transferable tactile transformers for representation learning across diverse sensors and tasks," in *8th Annual Conference on Robot Learning (CoRL)*, 2024, *arXiv:2406.13640*.